Article in Press: JJEES 16(2), June 2025.
This article has been accepted for publication and will appear in the upcoming issue. The final published version will be available through the journal website after copyediting, typesetting and proofreading.

Geological Structures Assessment in Wadi Hagul, Northwestern Gulf of Suez, Egypt, Using Gravity and Magnetic Techniques

Mahmoud S. Etman[1, 2*], Abdel-Monem S. Mohamed[1], Salah Saleh[1], Sayed A. Mohamed[3] and Karrar O. Fergawy[2]

[1]National Research Institute of Astronomy and Geophysics, Helwan, Cairo, Egypt
[2]Department of Geology, Faculty of Science, Aswan University, Aswan, Egypt
[3]National Authorities for Remote Sensing and Space Science (NARSS), Cairo, Egypt

Received on November 2, 2024, Accepted on January 11, 2025

Abstract

Wadi Hagul, an overlooked geological site in the northwestern region of Egypt's Gulf of Suez, is undergoing investigation through gravity and aeromagnetic measurements to ascertain the subsurface structure and foundational strata. Aeromagnetic and gravity-based prospecting techniques yield useful information about the region. The total aeromagnetic intensity (TMI) was derived by reducing the aeromagnetic data to the north magnetic pole (RTP). Maps, depicting Bouguer variations, were generated from corrected gravity data. Filtering approaches identified local anomalies and assessed the depths of both deep and shallow locations using radially powered spectrum integration. The depths of anomalies varied from 1 km to 3 km for both magnetic and gravity data. Bouguer gravity and magnetic data produced two-dimensional (2D) models and depth maps of the basement surfaces, indicating depths ranging from 300 m to 10000 m. The data analysis disclosed structural tendencies in various orientations (NE-SW, E-W, and NW-SE). Ten two-dimensional models demonstrated a deepening of foundation rocks in the center and southwestern regions. Employing forward 2D modeling alongside a structural map derived from the tilt derivative filter and Euler deconvolution solution, we generated a preliminary basement terrain map

* Corresponding author's email address: mahmoud.etman@nriag.sci.eg

indicating diverse depths and tectonic activity in the central and southern regions of Wadi Hagul. Crustal thickness increases in the central and southwestern areas while decreases in the northeastern and southeastern directions.

Keywords: Wadi Hagul; 2D Modeling; Crustal Structure; Bouguer Anomaly; RTP; Data Processing.

1. Introduction

The Wadi Hagul region includes the El Galala El Bahariya plateau and the mountains of Ataqa, Kaheilyia, Abou Treifiya, and Akheider. It is situated near the Cairo-Sokhna and Suez-Sokhna thoroughfares. The Gulf of Suez and the coastline area serve as habitats for wadis. Research suggests various migration phases from the Neogene to the late Miocene. The Red Sea formed as the Arabian Plate moved northward along the Gulf of Suez (Bosworth, 2015). Seismic activity has migrated to the Jubal Island area at the Gulf of Suez entrance, conforming to regional structural patterns (Roberts et al., 1988). The WNW to NW tectonic trend indicates active faulting, with earthquakes predominantly occurring on faults aligned WNW-ESE to NW-SE within extensional stress regimes (Abd El-Aal et al., 2019). Human activities can worsen soil compaction, leading to increased movement and tremors in areas that were previously less affected (Etman et al., 2024). Gravity and Magnetic (GM) techniques are utilized to ascertain structural patterns and evaluate crustal thickness, employing regional-residual isolation and Tilt Derivative (TDR) filters to delineate tectonic processes influencing the basement surface and sedimentary strata (Gaber et al., 2022). A crustal structure model was developed utilizing the forward modeling technique (GM-System) over ten profiles.

The depth of the basement was assessed utilizing 3D Euler deconvolution and 2D profiles. Aeromagnetic and Bouguer gravity data were analyzed to obtain insights into the structural

Article in Press: JJEES 16(2), June 2025.
This article has been accepted for publication and will appear in the upcoming issue. The final published version will be available through the journal website after copyediting, typesetting and proofreading. ©2025 JJEES.

characteristics and basement depths of the region for optimal planning. This work utilizes Bouguer gravity and reduction to North Magnetic Pole (RTP) aeromagnetic data to further our comprehension of Wadi Hagul's geodynamic evolution by delineating subsurface structures and basement relief in tectonically active regions. Figure 1 presents a location map of Wadi Hagul, including a geodetic network, fault lines, and seismic occurrences in the time period from 1950 to 2023.

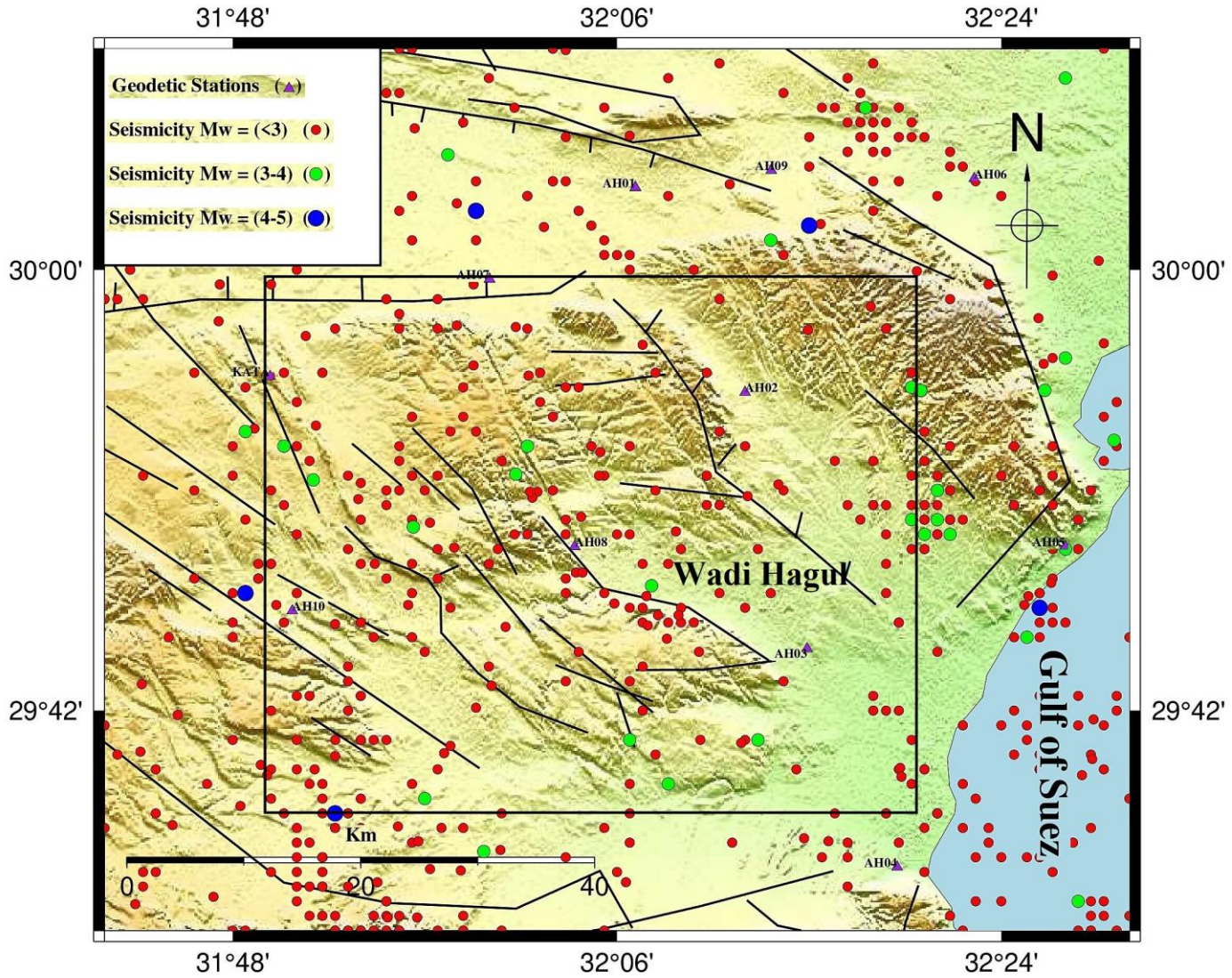

Figure 1: Location map showing Wadi Hagul, the geodetic network, and seismic events and highlighting fault lines in the investigated region.

2. Geologic Setting

The area encompasses a variety of rock types from the Jurassic to Quaternary eras, as shown by prior studies. The predominant rock units are strata from the Middle and Upper Eocene, Miocene, and Quaternary eras (Hassan, 2008). The Jurassic phase is characterized by multicoloured sandy rocks interspersed with layers of siltstone and clay. The Cretaceous series in the area has three distinct units: chalky limestone, Galala, and Malha. Eocene formations are prevalent in Gabal El-Galala El-Bahariya, Gabal Ataqa, Um Zeita-Kahallya, and Akheider-Rammlyia. The Eocene strata, mostly composed of carbonates interspersed with various quantities of clastic, constitute the stratigraphic series (Salem, 1988). Nonconformity distinguishes late Eocene layers from Oligocene and Miocene deposits. The Oligocene rocks are divided between lower variegated strata (sandstone and flint gravel) and top basalt layers of the Gabal El Ahmer formation, together with dolerite intrusions (Salem, 1988), (El-Enain et al., 1995). The Miocene sequence forms the Sadat, Hommath, and Hagul Fformations. In the Upper Miocene, the Hagul formation, mostly consisting of carbonate and sandstone, was formed (Abdallah, 1993), (O'Connor et al., 1990).

The Upper Miocene strata consist of 45-meter-thick argillaceous and calcareous sandstone, situated above these layers. The base of the water well has a thin stratum of limestone, sandstone, and clay, indicative of the Middle Miocene epoch. The region's intricate structural configuration is shaped by the Syrian Arc System and the Gulf of Suez Rift, leading to faulting, bending, and anomalies. Four tectonic episodes have been recognized as responsible for structural deformations: The Upper Oligocene, Upper Miocene, Lower Miocene, and After-Miocene epochs. The Pliocene sediments consist of gravels formed from a combination of flint and limestone, usually embedded in a sandy matrix. The Quaternary sediments, about 4 meters in thickness, consist of wadi deposits, sand, and gravel.

The subsurface stratigraphy of the study area was established using data from boreholes conducted by Egypt's Geological Survey in 1999. The topographical and structural characteristics of the Hagul were mostly influenced by the first two occurrences, resulting in more deformation compared to subsequent events by (Abd Allah et al., 1965). Recent and paleo-earthquakes have created geological deformation patterns in the Wadi Hagul region and its vicinity, retaining sedimentary strata. The examination of several data types indicates that the Hagul fault zone mostly governs the average depth of earthquakes in Wadi Hagul, ranging from 1 to 35 kilometres into the Earth's upper crust. The study region and its vicinity include a moderate topography characterized by many hills and small mountains. The elevation progressively ascends westward, merging with the Eocene limestone plateau in the central region of the northern Eastern Desert by (Abd Allah et al., 1965). The area between Gebel Ataqa and the Northern Galala Plateau links the Cairo-Suez region to the Gulf of Suez. Various fault types impact the Eocene and Miocene strata. NNW-SSE faults are often identified as gravity faults, distinguished by intermediate throw length ratios, significant throws, and shallow dip angles. The faults impacting the Eocene limestone plateau delineate prominent wadis, including Wadi Hagul and Wadi Hommath. East-West faults are characterized by moderate lengths, significant throws, intermediate throw-to-length ratios, and steep dip angles. They originated in the late Eocene and continued into the Oligocene (Salem, 1988). Faults classified as WNW-ESE exhibit moderate displacements, minimal throw length ratios, and steep dip angles. They are mostly located around Gebel El-Galala El-Bahariya and Gebel Ataqa, inside the low hilly landscape. Tectonic joints in this region are oriented northeast-southwest, north-south, and northwest. The region has seen considerable faulting, some folding, and non-depositional conformities. Previous studies by (Abdallah, 1993), (Safei El-Din, 1988). (Youssef et al., 2003) have examined the geological formations

of the Wadi Hagul area. Figure 2 illustrates the composite stratigraphic column for the investigated region and its adjacent areas.

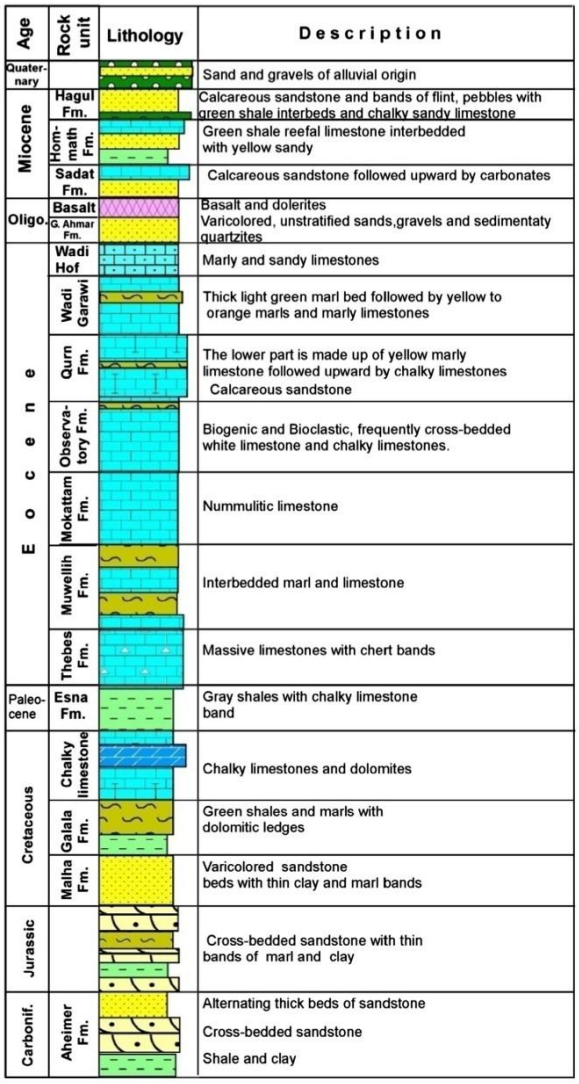

Figure 2: A modified and synthesized stratigraphic column of the study area (Araffa et al., 2017).

3. Material and Methods

The total field intensity (TF) magnetic and Bouguer gravity datasets are important research datasets. The magnetic method is recognized as one of the most often used geophysical methods for exploring the Earth's interior. It aids in the examination of many

exploration obstacles, including horizontal geomagnetic oscillations from the Earth's crust to the uppermost of the globe. This technique employs differences in subsurface attraction to detect changes in the Earth's magnetic field (Hinze et al., 2013). In highly conductive materials, the dissipation of eddy currents (secondary magnetic fields) occurs at a much slower rate compared to low-conductivity materials (Al-Amoush et al., 2017).

The aeromagnetic data for the area was obtained from a total intensity magnetic map (TIM) digitized at a resolution of 1:50,000. In 1983, the Egyptian Geological Survey and Mining Authority (EGSMA) commissioned the West Geophysical Service of America's Aero Service Branch for an investigation. The flight lines were positioned 120 meters above the Earth's surface, with a separation of 1.5 km in the NE-SW (45°/225°) direction and 5 km in the NW-SE (135°/315°) orientation. The magnetic field strength in the area was recorded at 41,742 nano Tesla (nT), with an average inclination and declination angles of 39.5 N and 2.0 E, respectively (A. service, 1984).

Two drilled wells were used to verify the precision of the modeled profiles. Figure 3 illustrates the Total Magnetic Intensity (TMI) map of the study area. Subsequently, to account for the effects of oblique magnetization, the TMI data were reduced to the pole (RTP) with the methodology outlined in (Baranov et al., 1964). The power spectrum curve of the RTP magnetic data was examined to detect localized and enduring magnetic anomalies. The energy spectrum graph exhibited two linear segments corresponding to shallower and deeper magnetic fields (Dosoky et al., 2023). There are established processing steps for interpreting magnetic data (Sundararajan et al., 2022). Edge detection methods (EDT) were used in a qualitative analysis of the data to identify patterns and correlations. Multiple EDTs, such as tilt derivative (TDR), Euler deconvolution (ED), and vertical derivative (VDR), were used in the analysis. Prior studies have similarly used EDT to delineate fundamental

structural characteristics (Oguama et al., 2021), (Basantaray et al., 2022). The quantitative analysis included magnetic depth estimate techniques including Power Spectrum Analysis (Spector et al., 1970). Euler Deconvolution (ED) by (Thompson et al., 1982), (Reid et al., 1990) and 2D Magnetic Modeling (Talwani et al., 1964).

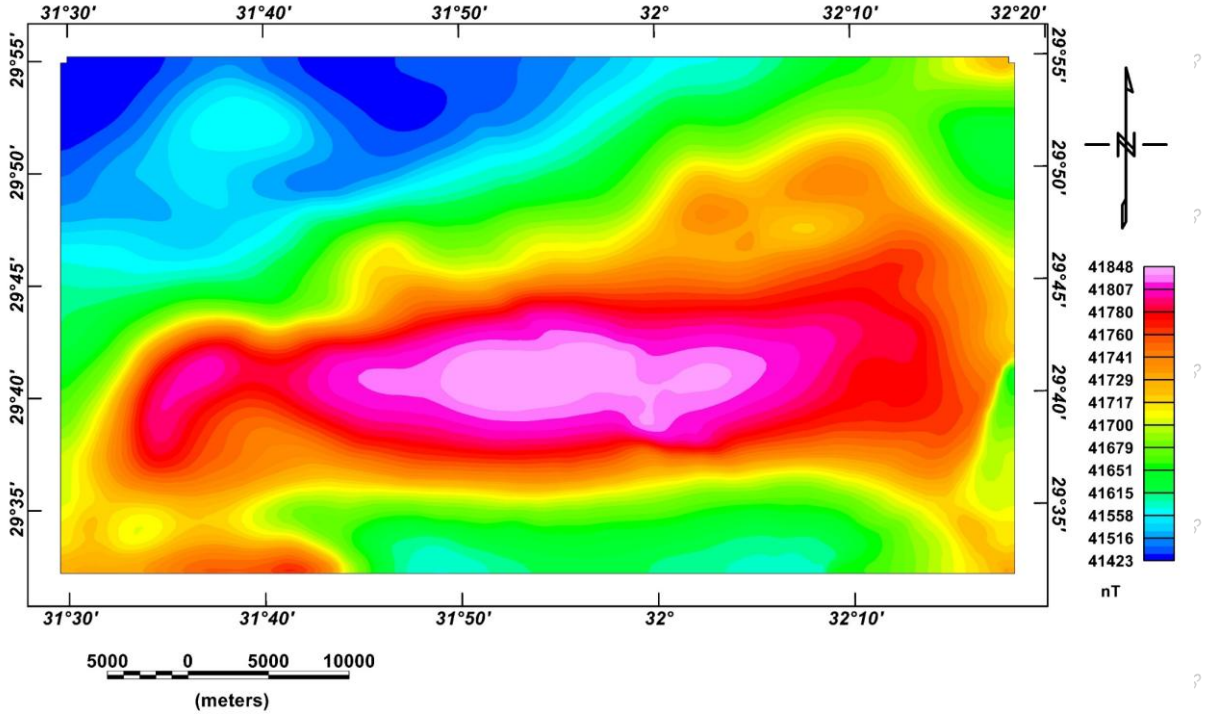

Figure 3: The total magnetic intensity (TMI) of the investigated region.

The RTP aeromagnetic and gravity measurements underwent comprehensive processing and enhancement using the Oasis Montaj software version 7.0. Gravity prospecting was conducted in the area due to its cost-effectiveness and non-invasive nature. This method is passive and does not require external energy input to collect data (Numan et al., 2019). The gravity method is used to detect fluctuations in the Bouguer field caused by subsurface density changes. This approach is essential for geological study, including mapping near-surface voids, evaluating metallic ore deposits, defining salt formations, and monitoring variations in volcanic fluid and gas compositions. It is used in regional Earth characterization to ascertain crustal structures, pinpoint prospective places for resource exploration, and

formulate investigative models (Hinze et al., 2013). In 1984, the General Petroleum Company created a Bouguer anomaly map at a scale of 1:200,000, with a contour interval of 1 mGal, an observation spacing of 1000 m, and a line spacing of 5000 m (EGPC, 1984).

The standard values of 2670 kg/m^3 and 0.3086 mGal/m were used to implement the Bouguer and Free-Air corrections, correspondingly. Gravity measurements are affected by elevation, density, and crustal composition. Regional Bouguer anomalies provide insights into isostatic equilibrium patterns and mass boundary fluctuations throughout the crust and upper mantle (Tealeb et al., 1986). Recent studies demonstrate a significant link among Bouguer anomalies, surface topography, and crustal thickness (Woollard, 1959), (Pick et al., 1973) and (Riad et al., 1985). Nevertheless, it is crucial to acknowledge that gravity measurements alone cannot conclusively ascertain the density distribution in the planet's deepest regions (Tealeb et al., 1986). The Gravity and Magnetic (GM) dataset underwent regional-residual separation analysis to distinguish anomalies caused by shallow geological factors from those arising at greater altitudes (Gaber et al., 2020). In this process, the identified field is subtracted from the regional field to get the local anomaly. Residual variations, stemming from shallow origins, have steep gradients and elevated frequencies, whereas regional anomalies are often extensive and smooth, indicative of their connection to deeper and bigger formations (Bassett et al., 2015). Residual anomalies have significance in geophysical exploration. The remaining components are isolated using various procedures, and a reliable method to ascertain the depths of different Gravity and Magnetic (GM) prospects characterized by varying densities or magnetic susceptibilities is via the analysis of the radial energy spectrum of (GM) data. Depth estimate findings are essential for measuring sediment thickness in sedimentary basins. The structural index (SI) of (0.5) for magnetic data and (1) for gravity data is used in the Euler method for identifying gravity and magnetic

anomalies. Faults or contacts at different depths within the research region are delineated by Euler deconvolution. The suitable SI value is contingent upon the source geometry, with values of two for spheres, one for horizontal cylinders, zero for faults, and negative one for contacts.

A structural index of zero or one is advised for identifying gravitational anomalies. Optimal results are achieved for SI = 0.5 and 1. Trends in structural elements are shown in rose diagrams derived from the gravity map, together with the Convolution of Euler using structural values of 1 (Araffa et al., 2018). Subsurface characteristics, including fault positions, depths, geological affiliations, lineaments, dykes, and sills, are ascertained by the 3D Euler approach. To do this, data on the causal components is necessary, measured by the structural index (SI). The SI numbers denote the degree of field displacements contingent upon the configuration of the source (Salem et al., 2008), (Eweis et al., 2022).

4. Results and Discussions

The overall magnetic intensity (Figure 3) and the accompanying RTP (Figure 4) exhibit a northward displacement in anomalies, which correlates with the magnetic inclination of the study area. There is an increase in the number of variants, a decrease in their aerial coverage, and an increase in their vertical relief. The RTP aeromagnetic anomaly shown in Figure 4 reveals a maximum reading of about 41850 nT in the north and a minimum decrease of around 41400 nT in the south (it is 41401 in the Fig. 4). The RTP map exhibits only positive anomalies characterized by diverse dimensions, forms, basins, lineation, and modest gradient extensions. The anomalies often manifest in the northeast, east-northeast, southeast, and northwest directions. The largest amplitude of 41,850 nT is seen in the northern region, whilst the lowest amplitude of 41,400 nT, directed ENE, is recorded in the southern area. The map illustrates significant magnetic anomalies in the northeastern, northwestern, and eastern

areas. The highest magnetic measurements fluctuate between 41,850 and 41,710 nT. A contrasted low magnetic anomaly is detected in the southern regions, with values ranging from 41401 to 41559 nT.

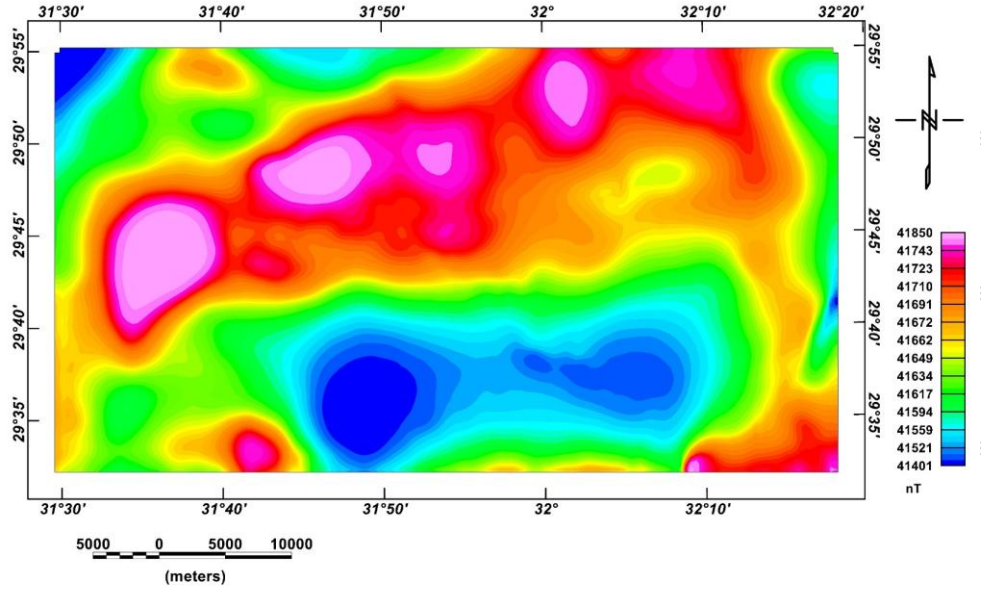

Figure 4: Reduction to Magnetic Pole (RTP) aeromagnetic map.

In the study region, the Bouguer anomalies (Figure 5) display four major anomalies. The western, northern, and southwest anomalies trend northwest with negative gravity values (-48 mGal), while the eastern anomaly trends northeast and the western anomaly with negative gravity values reaching -9 mGal. With amplitudes ranging from -48 to -9 mGal and a trend from west-northwest to east-northeast, four low anomalies basins or down-faulted blocks are indicated on the map. The significant negative anomaly in the eastern region, with an amplitude of -9 mGal, is associated with a high density.

Article in Press: JJEES 16(2), June 2025.
This article has been accepted for publication and will appear in the upcoming issue. The final published version will be available through the journal website after copyediting, typesetting and proofreading. ©2025 JJEES.

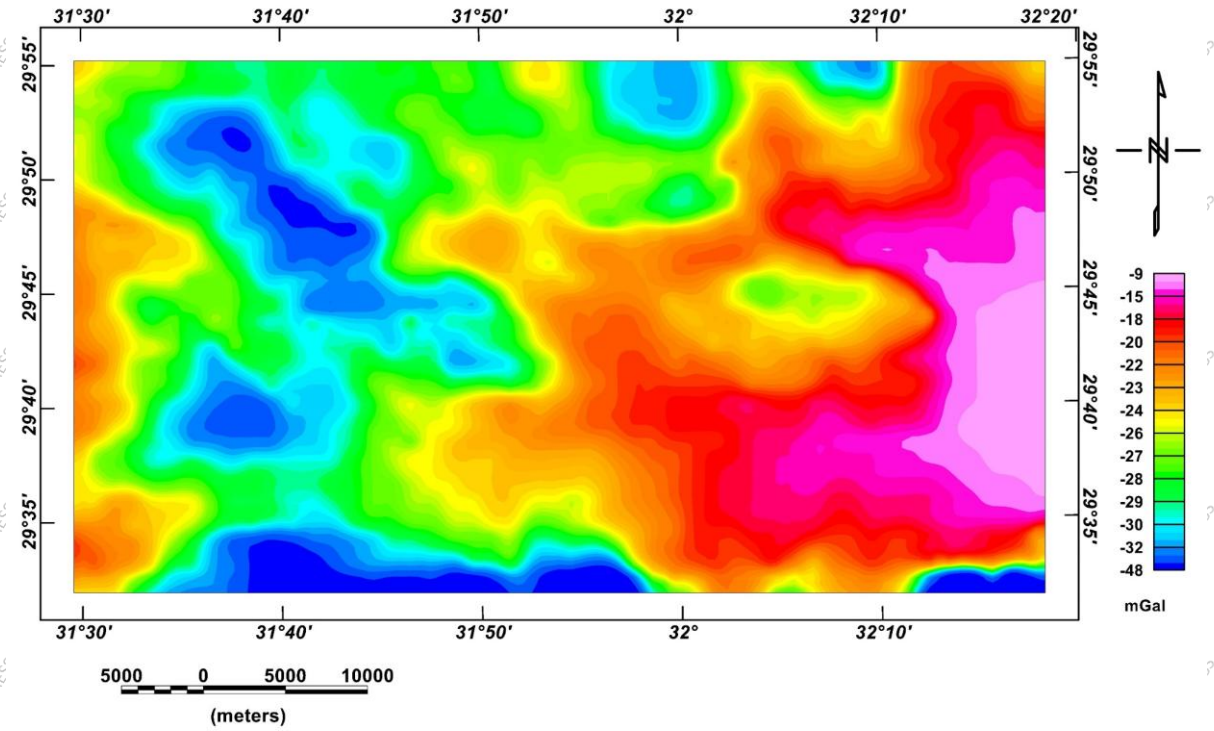

Figure 5: A Bouguer gravitational map of the investigation region.

Figure 6a illustrates the regional gravitational mapping, featuring a cut-off wave number of 0.023 Rad/m and four distinct Bouguer anomalies that range from -37 to -12 mGal. The low-pass magnetic and Bouguer maps presented in Figures 6a and 6b illustrate deep magnetic sources, indicating both positive and negative anomalies within the study area. Figure 6b presents a regional magnetic anomaly map that indicates the presence of buried correlated resources, characterized by magnetic intensity levels between 41,450 and 41,783 nT. In the illustrated region, low magnetic anomalies are predominantly found in the southern areas, while high magnetic RTP anomalies are concentrated in the northeastern and western sections. The subject exhibits an additional east-west trend in its central and southern regions, while most regional irregularities are oriented in the northeast-southwest and northwest-southeast directions, consistent with the Gulf of Suez pattern. A comparison of the regional map in Figure 6b with the RTP map in Figure 4 reveals notable similarities across most

regions, including central, northeast, and certain areas in the west, indicating the regional origin of RTP anomalies in specific locations.

After the removal of regional effects, the high-pass gravity and magnetic (GM) maps presented in Figures 7a and 7b reveal irregularities that suggest the presence of multiple causal GM entities at shallower depths. The high-pass Bouguer anomaly map reveals elongated anomalies with amplitudes ranging from -11 to 8 mGal in the ENE, WNW, and E-W orientations. Figure 7b illustrates a residual aeromagnetic anomaly pattern characterized by high frequencies, small wavelengths, and minimal magnetic variations, which delineate near-surface structures in the study area. Upon removal of the regional magnetic field, the local RTP map reveals dispersed low and high-frequency anomalies with amplitudes ranging from -117 to 110 nT., indicating significant northwest, north-south, east-west, and northeast trends. The Fast Fourier Transform (FFT) distinguishes between regional (low-frequency) and local (high-frequency) elements. The power spectrum is depicted in Figure 8, with gravity in Figure 8a and aeromagnetic analysis in Figure 8b. The analysis of the radially summed energy spectrum reveals a low wave number slope (green line), indicating deep sources, while high wavenumbers (blue line) imply shallow contributions. Long-wavelength aberrations from deep sources are represented on regional maps, with depths of 3000 m in the Bouguer measurements and the RTP dataset. Small wavelength anomalies from shallow sources are seen in the residual maps, suggesting depths of 1000 m in the Bouguer data and the aeromagnetic measurements.

Article in Press: JJEES 16(2), June 2025.
This article has been accepted for publication and will appear in the upcoming issue. The final published version will be available through the journal website after copyediting, typesetting and proofreading. ©2025 JJEES.

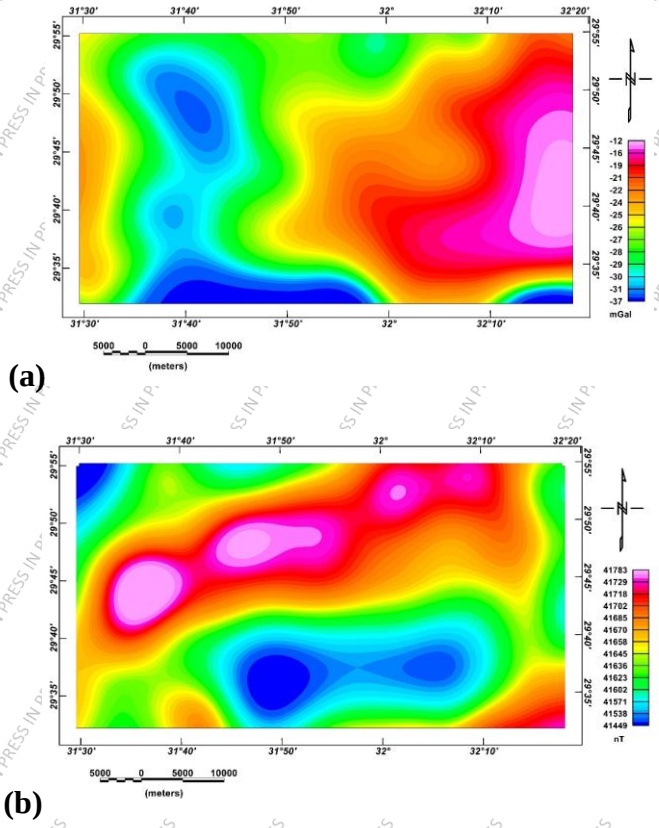

Figure 6: Low-pass filters for regional analysis on both a) the Bouguer and b) RTP anomaly maps, with a 0.023 cycles/km cut-off wave number.

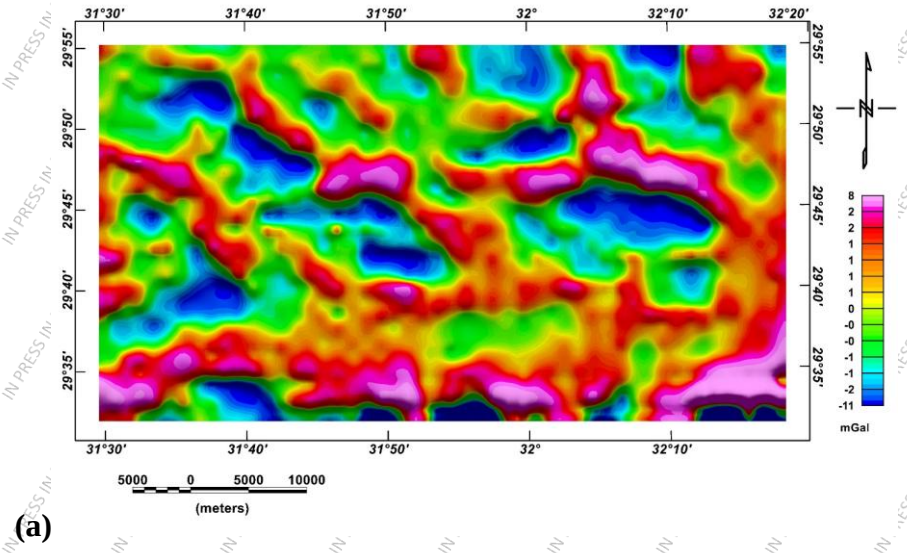

Article in Press: JJEES 16(2), June 2025.
This article has been accepted for publication and will appear in the upcoming issue. The final published version will be available through the journal website after copyediting, typesetting and proofreading. ©2025 JJEES.

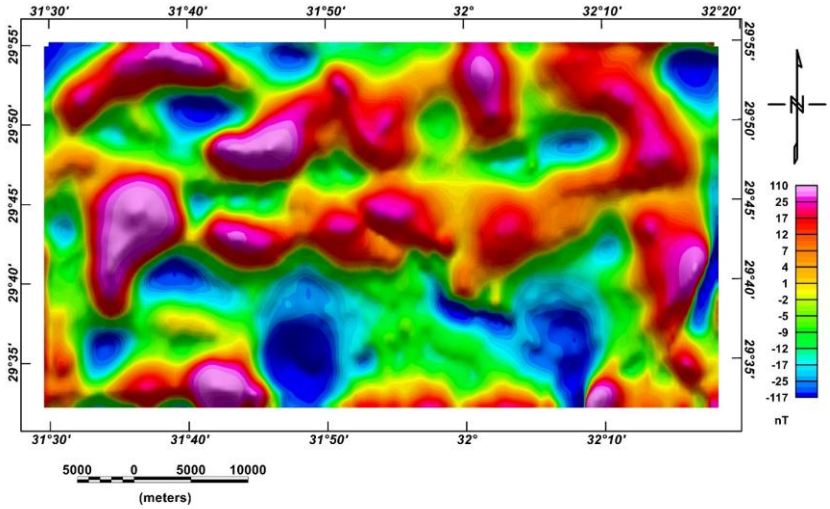

(b)

Figure 7: High-pass residual filters are applied to both a) the Bouguer and b) RTP anomaly maps, with a 0.023 cycles/km cut-off wave number.

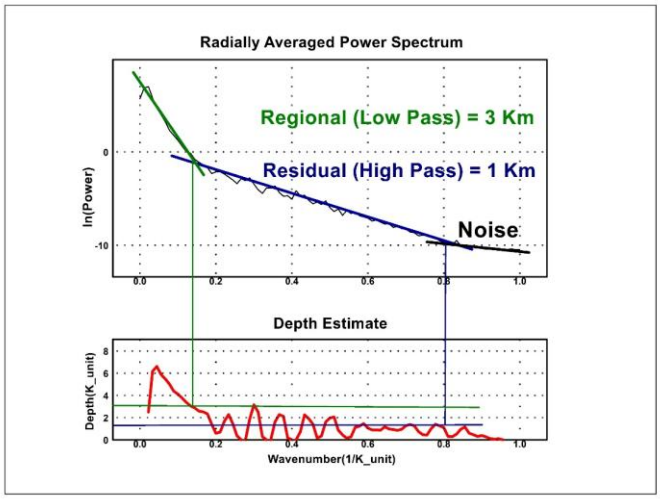

(a)

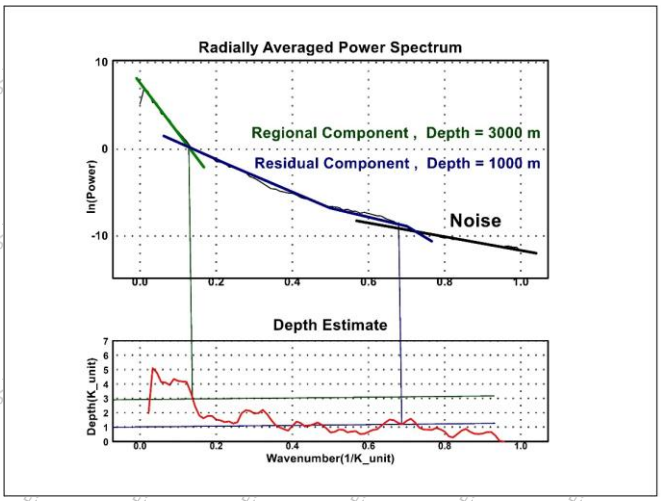

(b)

Figure 8: Two types of data are analysed using radial power spectrum evaluation and depth estimation: a) Reduced-to-pole (RTP) aeromagnetic data and b) Bouguer gravity measurements.

By considering the lateral slope, the Tilt Derivative (TDR) approach corrects the vertical variation in prospective measurements (Miller et al., 1994). The TDR gravity map (Fig. 9a) highlights uplifted and down-faulted block boundaries. The TDR magnetic map (Fig. 9b) shows distinct boundaries with varied dimensions, shapes, and orientations of magnetic sources, which differ from the gravity map. The depths of the magnetic boundaries appear shallower than those of the gravity boundaries. TDR amplitudes are positive above the point of origin, null at its border, and negative outside the body's limits. The amplitudes vary from $-\pi/2$ to $+\pi/2$. The path along which the contour measurements collapse indicates the downthrown opposite faults. This method was used to identify the fault elements, as shown in Figure 9.

In Figure 10, a rose diagram illustrates trend orientations derived from the tilt derivative (TDR) in aeromagnetic data (RTP). The linear anomalies or faults in the Rose diagram display NW-SE in major trend and E-W, N-S, NE-SW in minor trends. In the reduced-to-pole aeromagnetic analysis, the limits of the likely basin-like structure in the south and the possibly raised basement block in the north are defined by the zero-point outlines of the tilt derivative (TDR). Many regular faults, which run along the edges of the basement and the sedimentary nature basin, influence and contribute to the formation of these geologic features. The 3D Euler approach on aeromagnetic fields was utilized to identify the lineaments and faults in the focal region, and Bouguer analysis was used to establish their positions and depths.

Article in Press: JJEES 16(2), June 2025.
This article has been accepted for publication and will appear in the upcoming issue. The final published version will be available through the journal website after copyediting, typesetting and proofreading. ©2025 JJEES.

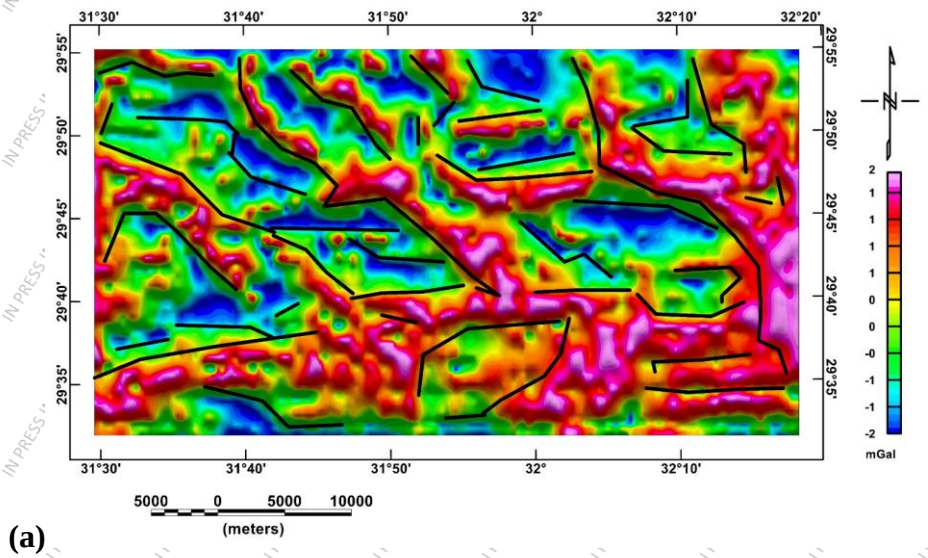

(a)

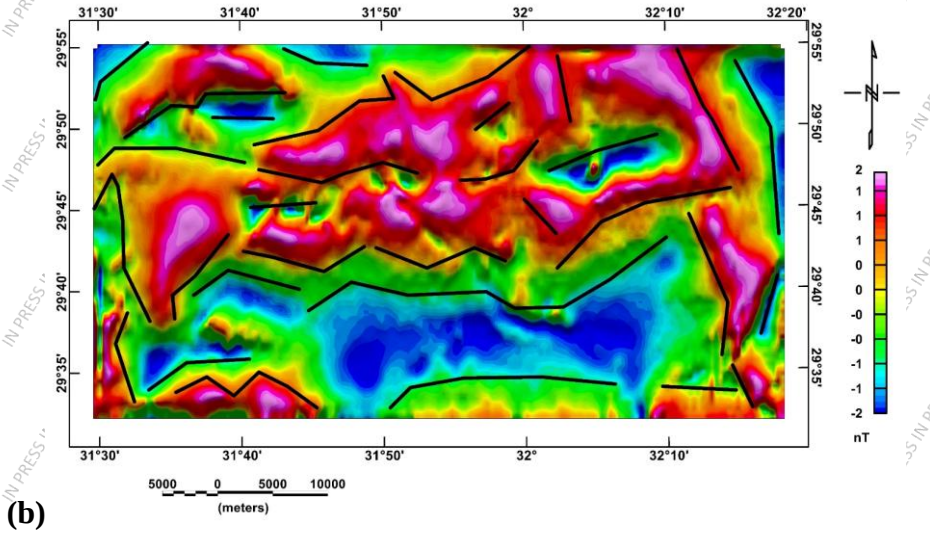

(b)

Figure 9: a) Gravity anomalies in the TDR map, b) Unusual magnetic fields in the TDR.

Article in Press: JJEES 16(2), June 2025.
This article has been accepted for publication and will appear in the upcoming issue. The final published version will be available through the journal website after copyediting, typesetting and proofreading. ©2025 JJEES.

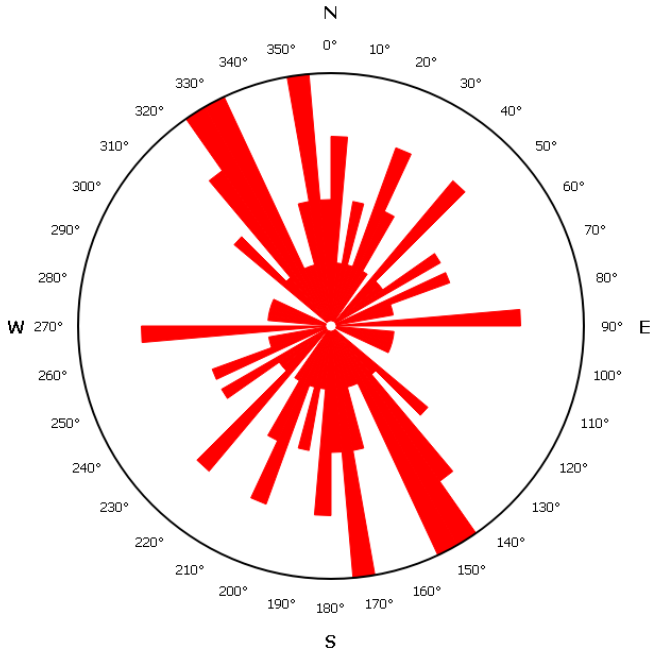

Figure 10: The trends in the Rose chart is extracted from the Tilt Derivative (TDR) aeromagnetic data (RTP).

Figure 11 shows the findings for the analysis of the region's Bouguer observations using the Euler methods. With the Bouguer map, lineaments, geological contacts, dykes, faults, and sills could all be precisely located (Figure 11) with SI = 1. According to the results of Bouguer data, the depth ranges from less than 500 meters and reaches a maximum of 3500. Trends in the east-west, east-northeast, and west-northwest directions are shown by the negative anomalies, while linear anomalies or faults show an east-west and NW-SE in major trends and E-W, NE-SW, N-S and WNW in minor trends as depicted in Figure 10 and 12. The Rose diagram (Figure 12) displays the principal orientation structure's NW-SE orientation and NE-SW, NW-SE in minor trends.

Article in Press: JJEES 16(2), June 2025.
This article has been accepted for publication and will appear in the upcoming issue. The final published version will be available through the journal website after copyediting, typesetting and proofreading. ©2025 JJEES.

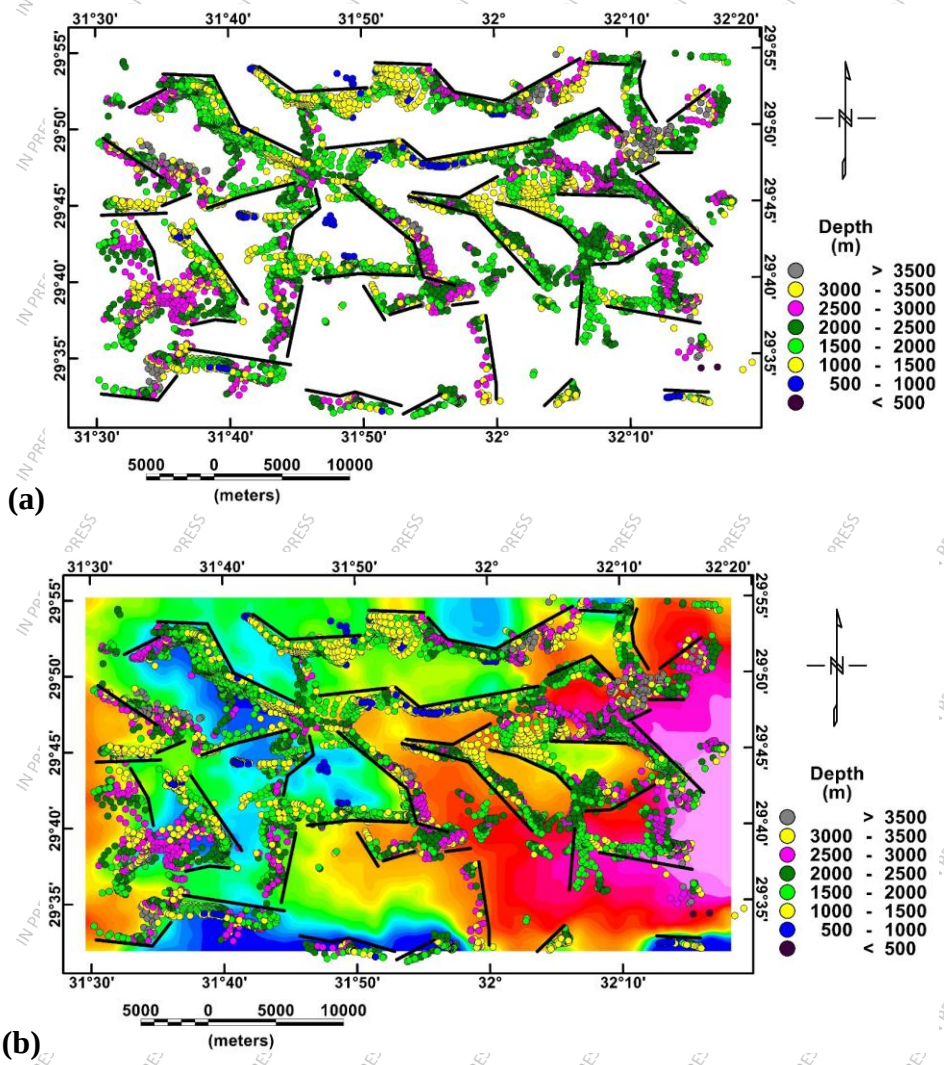

Figure 11: The Euler Deconvolution solutions map for SI (1) superimposed on the Bouguer anomalies pattern defines the position and depth of the faults.

Article in Press: JJEES 16(2), June 2025.
This article has been accepted for publication and will appear in the upcoming issue. The final published version will be available through the journal website after copyediting, typesetting and proofreading. ©2025 JJEES.

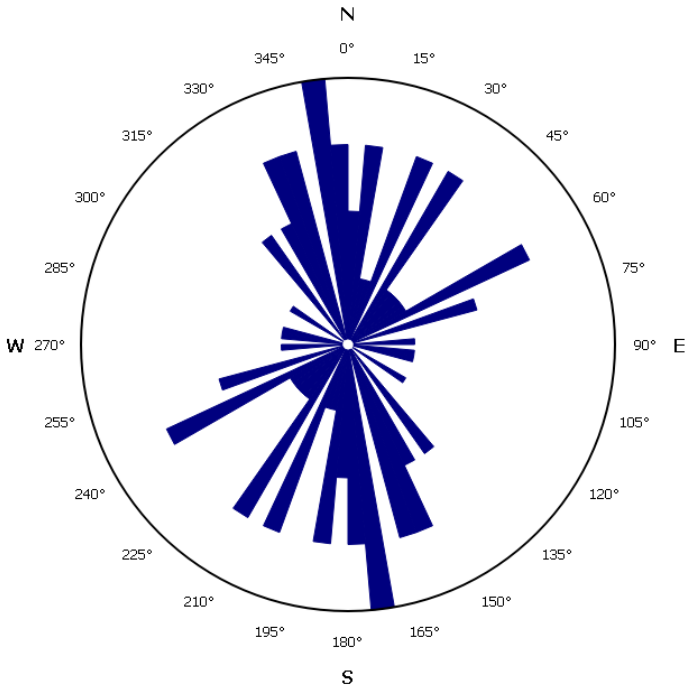

Figure 12: The trend of the patterns is extracted from the Euler Bouguer map is represented as a Rose diagram.

Profiles P1 through P10 are distributed across all regions (Figure 13). Figure 13 illustrates two wells that intersect the basement surface. Ten gravity and magnetic models were developed along profiles P1 to P10 utilizing the GM-SYS tool in Geosoft Oasis Montaj to analyze the composition and structures of the basement. Two layers of sedimentary material were produced, exhibiting densities of 2.67 g/cc and 2.2 g/cc, and the magnetic field equals zero magnetic susceptibility in this layer. The magnetic susceptibility of basement rocks was measured at 0.00776 (Figure 14). Acidic rocks exhibit low magnetic susceptibilities, suggesting the existence of regional granitic basement layers, whereas basaltic rocks are linked to higher susceptibilities (Telford et al., 1990). The profiles depicted on gravity and RTP aeromagnetic charts cross regions exhibiting varying GM signatures and are oriented from south to north and westward, utilizing two reference wells (Figure 14). The modeling process entailed modifying depths, shapes, dimensions, and density contrasts to

Article in Press: JJEES 16(2), June 2025.
This article has been accepted for publication and will appear in the upcoming issue. The final published version will be available through the journal website after copyediting, typesetting and proofreading. ©2025 JJEES.

attain a close correspondence between observed and calculated gravity data. Two-dimensional models were created utilizing the Geosoft mapping system.

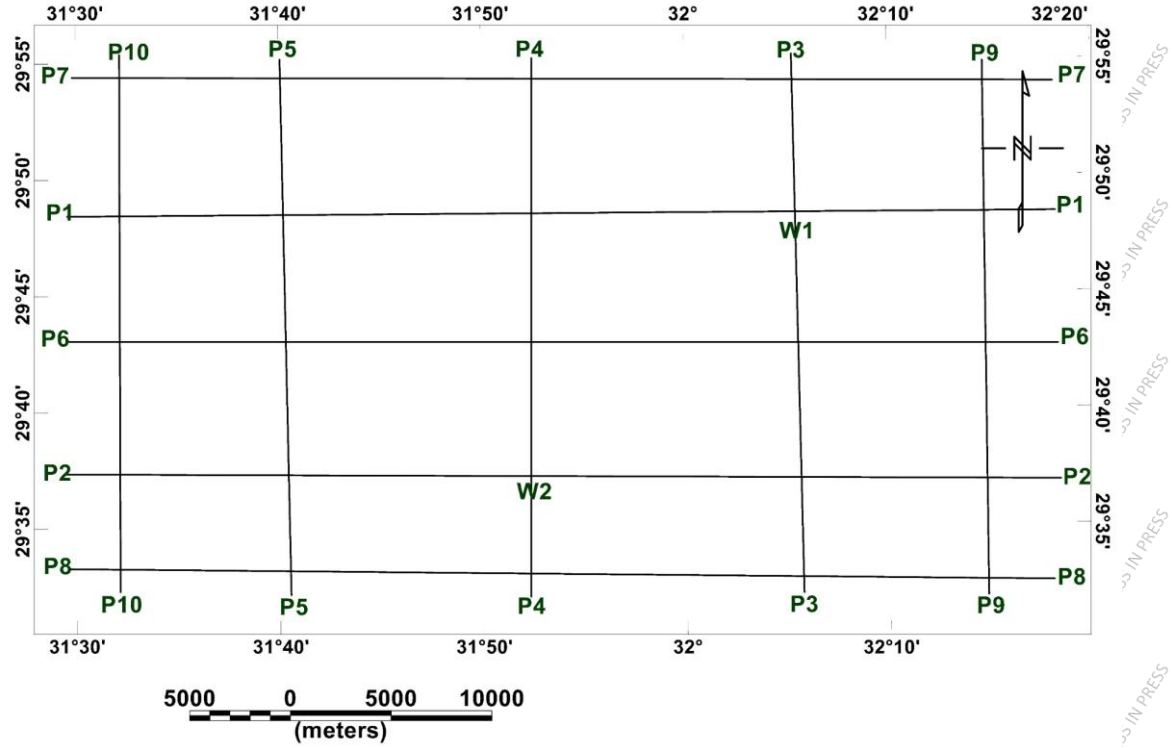

Figure 13: The base map displays the positions of the selected profiles for two-dimensional (2D) modelling of RTP and Bouguer gravity, along with the locations of the two well points.

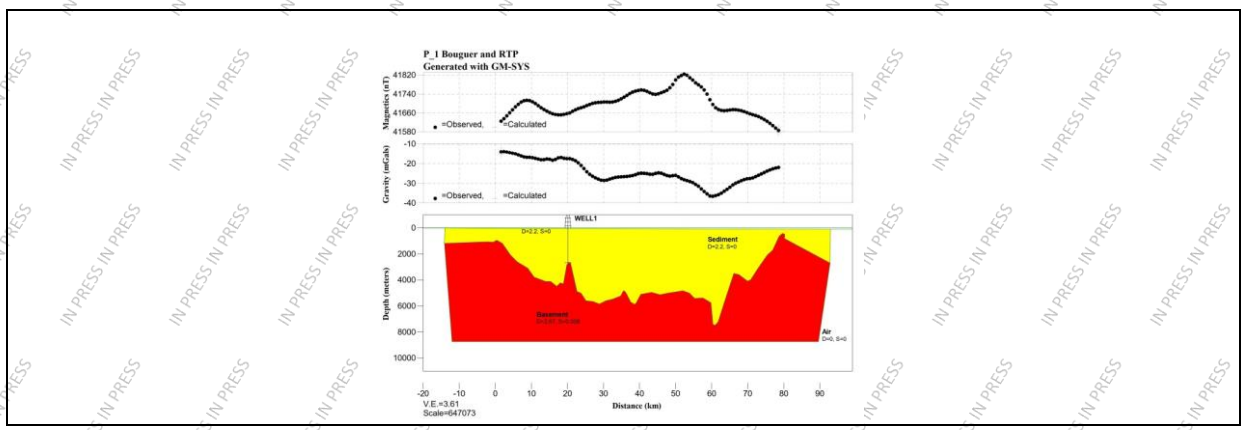

Article in Press: JJEES 16(2), June 2025.
This article has been accepted for publication and will appear in the upcoming issue. The final published version will be available through the journal website after copyediting, typesetting and proofreading. ©2025 JJEES.

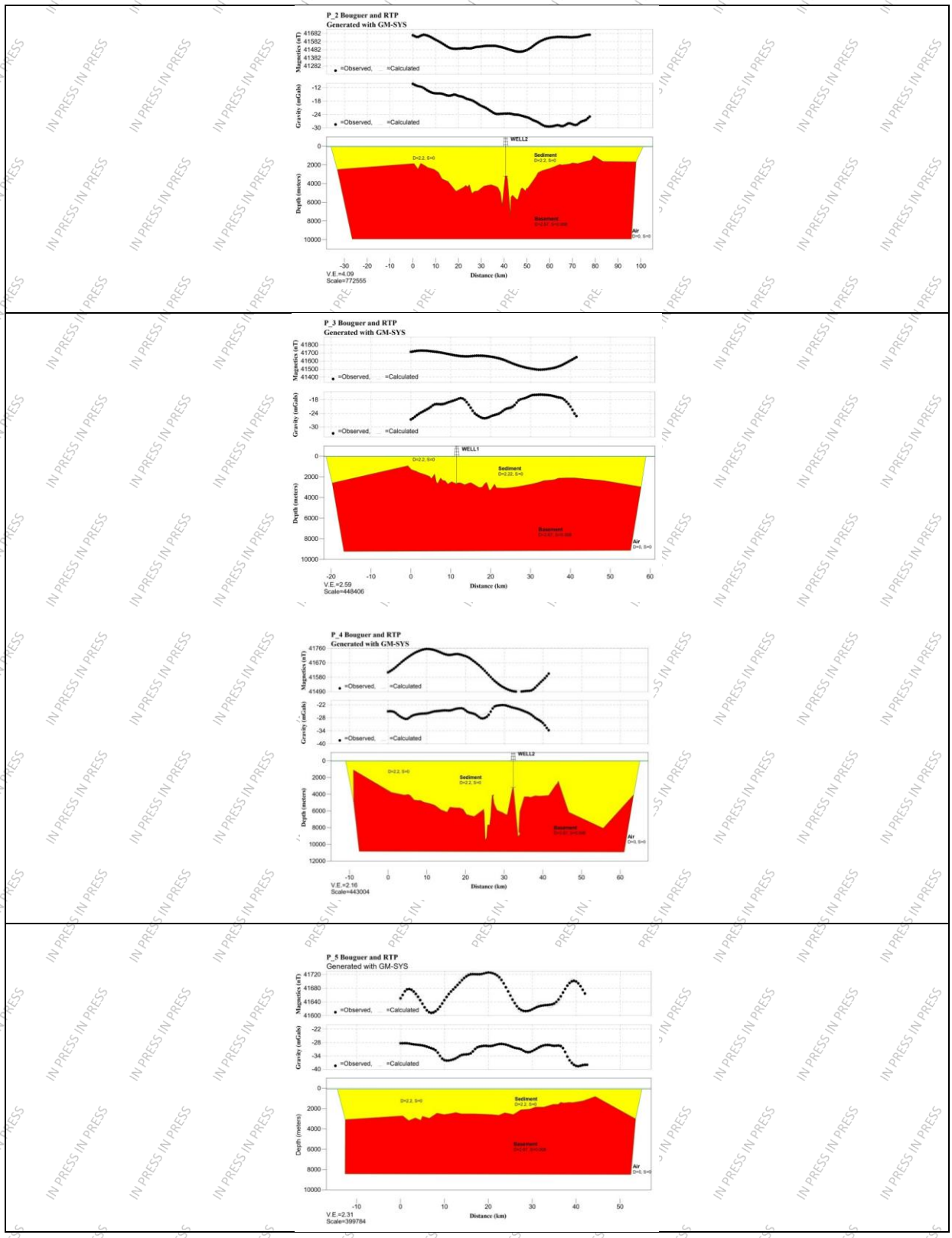

Article in Press: JJEES 16(2), June 2025.
This article has been accepted for publication and will appear in the upcoming issue. The final published version will be available through the journal website after copyediting, typesetting and proofreading. ©2025 JJEES.

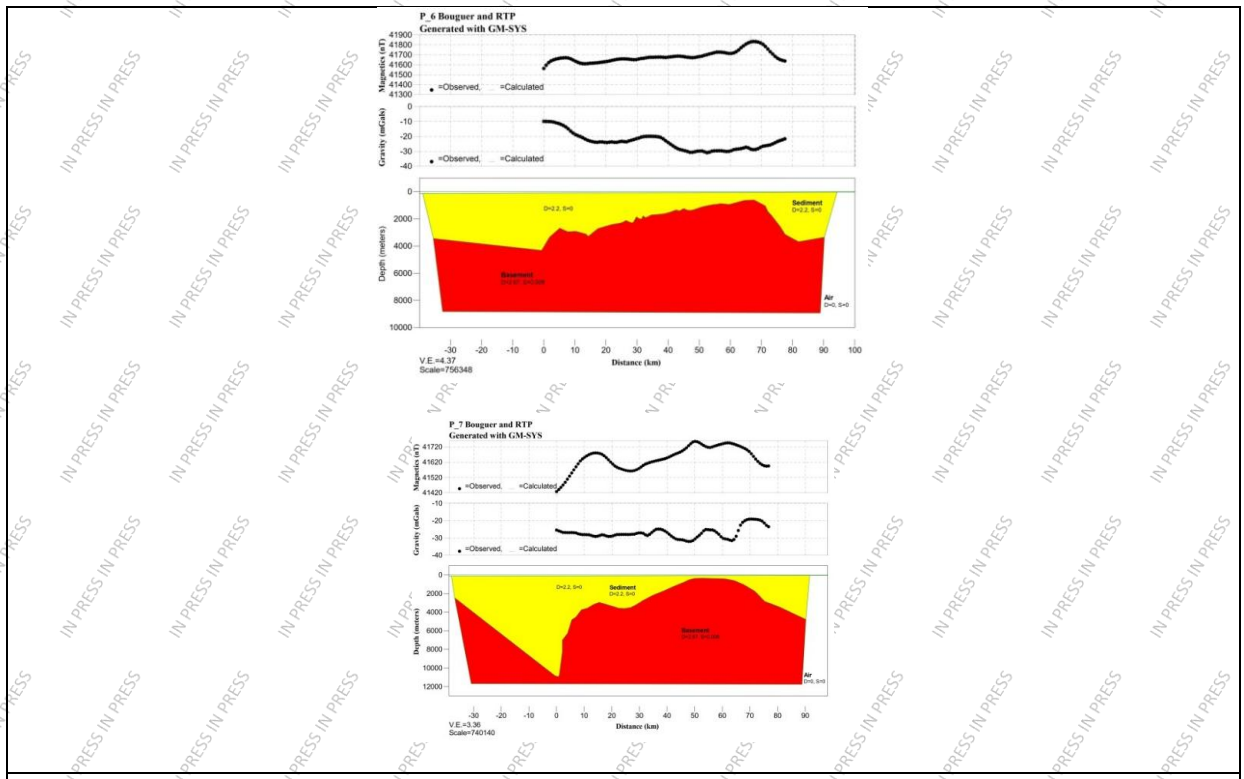

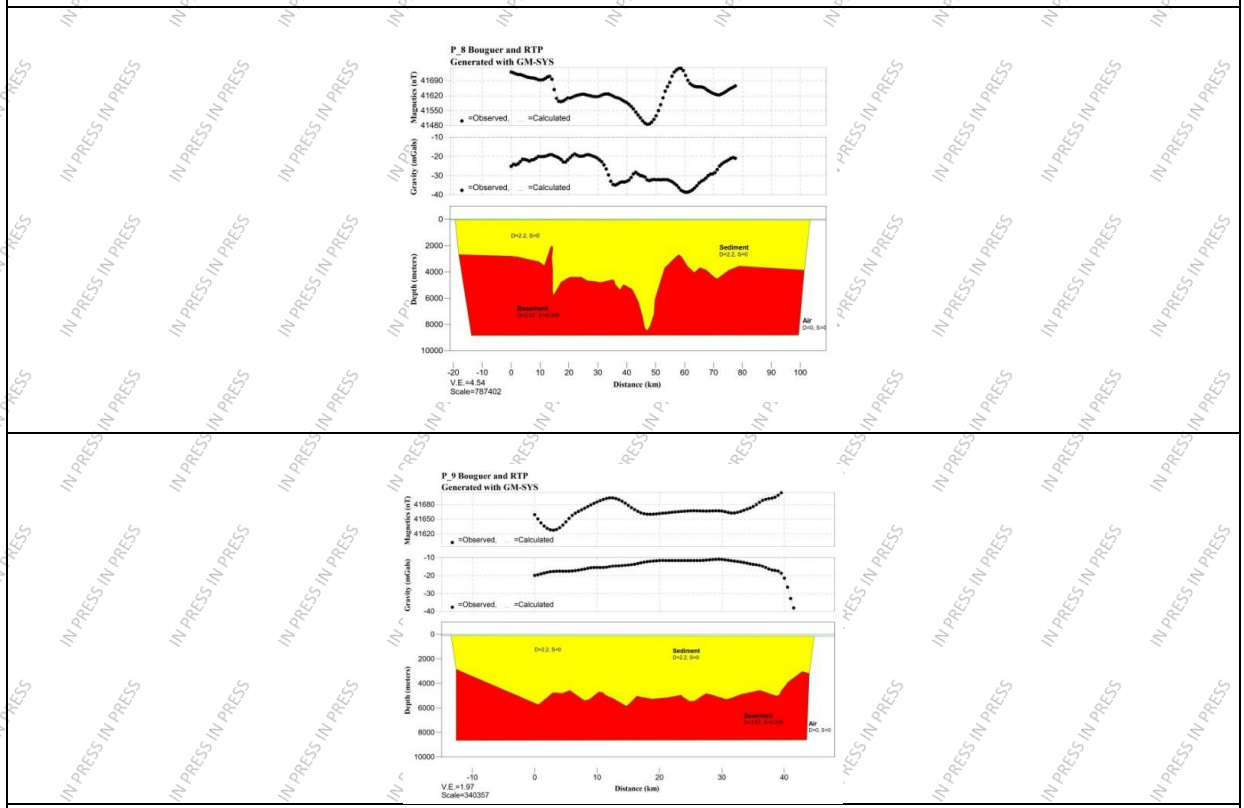

Article in Press: JJEES 16(2), June 2025.
This article has been accepted for publication and will appear in the upcoming issue. The final published version will be available through the journal website after copyediting, typesetting and proofreading. ©2025 JJEES.

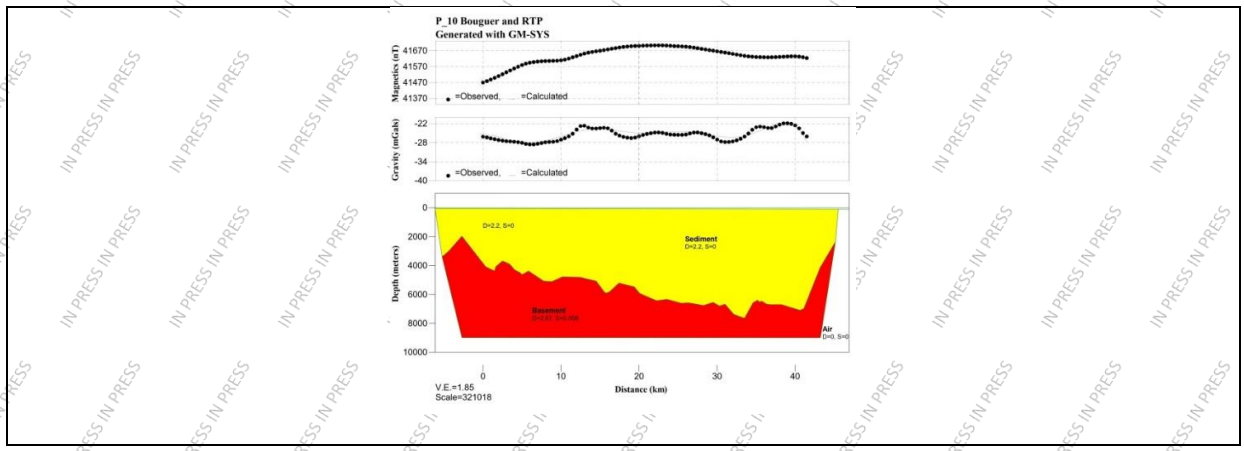

Figure 14: 2D gravity and magnetic model of profiles (P1:P10) of Wadi Hagul Area using reference depth's point.

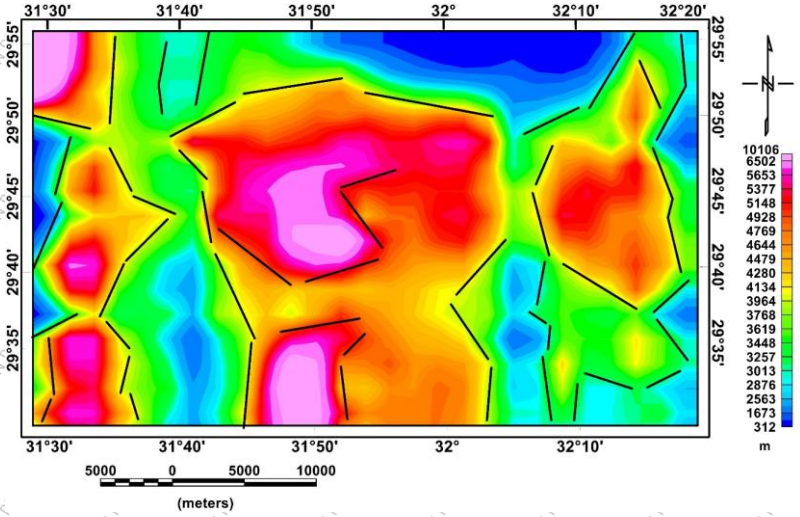

Figure 15: Relief map of the basement with lineaments in the study area.

The profiles indicated the existence of basement rock south of Wadi Hagul, with sedimentary thickness increasing in a northerly direction. The profiles were adjusted to reconcile observed and calculated data, with fitting errors between 0.1 and 3 percent. The densities of various rocks were assessed using magnetic and Bouguer measurements. The sedimentary cover and basement rocks were found to have average densities of 2.2 and 2.67 g/cm2, respectively, as determined through comparisons with prior research. Sequential modeling of the original magnetic and Bouguer data (Figure 14) produced more constrained interpretation results

compared to independent modeling of each dataset. The forward modeling parameters and the resulting anomalies were established (Bhattacharyya et al., 1965).

The anomaly observed analyzing along these profiles indicates a gravity field ranging from -9 to -48 mGal, characterized solely by negative anomalies. The magnetic field displays a central positive anomaly with a magnitude of 41,850 nT, corresponding to the peak depth of the well. A northward shift in the magnetic field is generally observed. Two wells constrain the basement depths and sedimentary thickness along these profiles (Figure 14). The modeled section indicates a sedimentary cover depth between 300 and 1000 meters. The modeled sections reached a depth of 10 km, spanning an approximate distance of 90 km, corresponding to the basement layer depth.

Geophysical methods are progressively employed in research concerning crustal, shallow, and deep structures, in addition to archeology, mineralization, geothermal, and hydrogeological investigations such as previous studies of the following., (Sehsah et al., 2022), (Pham et al., 2021), (Saada et al., 2021) and (Saada, 2020). Depth variations on the basement surface map are shown using well data and information from 10 two-dimensional Bouguer and RTP magnetic profiles. The basement surface maps were derived from 10 Bouguer and aeromagnetic RTP profiles (P1 to P10), with their positions shown in Figure 14. The basement relief map (Figure 15) indicates a depth of 300 m, with shallower areas located in the southeastern, southwestern, and northeastern regions, and the shallowest depths identified in the extreme north and southeast. Deeper basement strata, about 10000 m under sea level, are located in the northwestern, south, eastern and central regions of the study area. The bottom layers in the center and northwest regions of the study area are noted to be thicker. The geophysical observations compiled here may also aid in the comprehension of comparable systems in different areas (El-Kelani, 2020). The magnetic anomalies (41,400 to

41,850 nT) identified in this study are similar to those reported in the Gulf of Aqaba by (Gaber et al., 2022) (41,200 to 41,900 nT). These anomalies are believed to be caused by variations in basement rock composition and depth. Both studies highlight the impact of regional tectonic activities on the distribution of magnetic anomalies. The NW-SE and NE-SW structural trends observed in this study align with orientations described by (Gaber et al., 2022), underscoring the influence of tectonic fault systems on subsurface features.

The magnetic and gravity anomalies in this study align with the findings of (Saada et al., 2021), displaying comparable values in sedimentary basins characterized by NW-SE and NE-SW structural trends. The residual high-pass Bouguer and magnetic maps also mirror the patterns observed by (Saada et al., 2021), suggesting shallow sources and faulted blocks influenced by regional tectonic regimes. The Bouguer anomalies (-48 to -9 mGal) identified in this study are consistent with the results reported by (Gaber et al., 2020) in tectonically active areas characterized by thick sedimentary layers and faulted basement structures. The variations in basement depth (ranging from 300 to 10000 meters) are similar to those observed by (Gaber et al., 2020), indicating the influence of extensional tectonics and sedimentary processes.

5. Conclusions

Based on the Bouguer gravity and the RTP aeromagnetic data, considering the outcomes of the 2D for both aeromagnetic and Bouguer models, the following conclusions can be inferred:

- The basement section of the investigation area exhibits non-linearity, with depth variations from 250 to 9600 m, increasing towards the central and north-western regions.
- The structural elements in the region exhibit orientations in multiple directions,

including NNW–SSE, E–W, and NE-SW. A significant fault has been identified in the south-eastern part of this region.

- The region exhibits a typical continental crustal structure, characterized by a decrease in crustal depth toward the northeast and southeast. Moving Northward increases density for both the crust and the upper sedimentary section.
- The tectonic analysis indicates significant uplift in the north-western and central regions of the study area, as illustrated by the basement relief depiction.
- Crustal thickness decreases in the SE and NE regions of Hagul, while it increases towards the central area.
- This study identifies structural components and depths within layers through the application of 2D forward modeling, Euler deconvolution, and filtering techniques. A 3D model of gravity and magnetic data is necessary.

Author Contributions: Mahmoud S. Etman designed the study, gathered and evaluated the results, and authored the report. Abdel-Monem S. Mohamed participated in data gathering, manuscript preparation, and material creation. Sayed A. Mohamed contributed to data processing activities. Karrar O. Fergawy and Salah Saleh participated in data assessment and the formulation of findings. All contributors have reviewed and approved the last version of the paper.

Acknowledgment The authors wish to express their sincere appreciation to the Geodynamic Department, the NRIAG staff, and the NARSS team for their invaluable assistance in data collection.

Conflicts of Interest The authors declare no conflict of interest.

Funding The authors received no financial support for the research, authorship, and/or

publication of this article.

References

Abdallah, M. (1993). *Structural geology of the area between El Galala El-Bahariya and Gabal Okheider, Egypt* (Doctoral dissertation, Ph. D. Thesis, Ain Shams University, Cairo).

Abd El-Aal, A. E. A. K., Hagag, W., Sakr, K., Saleh, M., Abd El-Aal, A. E. A. K., Hagag, W., ... & Saleh, M. (2019). Seismicity, seismotectonic and neotectonics in Egypt. In The Geology of Egypt. Cham: Springer International Publishing. (pp. 375-413).

Al-Amoush, H., Al-Shabeeb, A. R., Al-Adamat, R., Al-Fugara, A. k., Al Ayyash, S., Shdeifat, A., & Rajab, J. (2017). The Use of GIS Techniques and Geophysical Investigation for Flood Management at Wadi Al-Mafraq Catchment Area. *Jordan Journal of Earth and Environmental Sciences*, *8*(2), 97-103.

Araffa, S. A. S., Mohamed, A. M., & Santos, F. M. (2017). Geophysical investigation in the Northwestern part of the Gulf of Suez, Egypt. *Egyptian journal of petroleum*, *26*(2), 457-475.

Araffa, S. A. S., El-bohoty, M., Abou Heleika, M., Mekkawi, M., Ismail, E., Khalil, A., & Abd EL-Razek, E. M. (2018). Implementation of magnetic and gravity methods to delineate the subsurface structural features of the basement complex in central Sinai area, Egypt. *NRIAG Journal of Astronomy and Geophysics*, *7*(1), 162-174.

A. service. (1984). "Final report on airborne magnetic/radiation survey in Eastern Desert, Egypt. Work Completed for the Egyptian General Petroleum Corporation (EGPC)," vol. Six volumes, Aero Service, Houston, Texas, USA.

Baranov, V., & Naudy, H. (1964). Numerical calculation of the formula of reduction to the magnetic pole. *Geophysics*, *29*(1), 67-79.

Basantaray, A. K., & Mandal, A. (2022). Interpretation of gravity–magnetic anomalies to delineate subsurface configuration beneath east geothermal province along the Mahanadi rift basin: a case study of non-volcanic hot springs. *Geothermal Energy*, *10*(1), 6.

Bassett, D., & Watts, A. B. (2015). Gravity anomalies, crustal structure, and seismicity at subduction zones: 1. Seafloor roughness and subducting relief. *Geochemistry, Geophysics, Geosystems*, *16*(5), 1508-1540.

Bhattacharyya, B. K. (1965). Two-dimensional harmonic analysis as a tool for magnetic interpretation. *Geophysics*, *30*(5), 829-857.

Bosworth, W (2015). "Geological evolution of the Red Sea: historical background, review, and synthesis," The Red Sea: The formation, morphology, oceanography and environment of a young ocean basin, pp. 45-78.

Dosoky, W., Elkhateeb, S. O., & Aboalhassan, M. (2023). Basement configuration and structural mapping using aeromagnetic data analysis of El Galala El Qibliya plateau area, Northeastern Desert, Egypt. *Modeling Earth Systems and Environment*, *9*(2), 2039-2051.

EGPC. (1984). "Bouguer gravity map of Egypt, Scale 1:500,000. Corporation Egyptian General Petroleum.,".

El-Enain, A., & FM, A. MM, & Ismail, AS (1995). Petrography, Geochemistry and Depositional History of the Eocene Rocks in the Area between Northern Galala and Gabal Ataqa, Western Gulf of Suez, Egypt. *Annals of the Geological Survey of Egypt*, *20*, 551-576.

El-Kelani, R. (2020). A Review of Gravity and Magnetic Studies in the Jordan Dead Sea Transform Zone. *Jordan Journal of Earth & Environmental Sciences*, *11*(1).

Etman, M. S., Mohamed, S. A., Saleh, S., Mohamed, A. M. S., & Fergawy, K. O. (2024).

Analyzing recent deformation in Wadi Hagul, Eastern Desert, Egypt, via advanced remote sensing and geodetic data processing. Journal of Applied Geodesy.

Eweis, A. M., Toni, M., & Basheer, A. A. (2022). Depicting the main structural affected trends by operating aeromagnetic survey in the western part of Koraimat-Alzafarana road and surround area, Eastern Desert, Egypt. *Modeling Earth Systems and Environment*, *8*(2), 2803-2816.

Gaber, G. M., Saleh, S., & Toni, M. (2022). Crustal thickness and structural pattern evaluation of Sinai Peninsula using three-dimensional density modeling with aeromagnetic and earthquake data. *Acta Geophysica*, *70*(2), 639-657.

Gaber, G. M., Saleh, S., & Toni, M. (2020). CRUSTAL STRUCTURE OF THE SINAI PENINSULA, USING GRAVITY DATA.

Hassan, S. M. (2008). Studying geological structures of Ayn-Sokhna area, north Eastern Desert, Egypt, by optimum utilization of data fusion techniques of some satellite image. *Faculty of science, Helwan University*, 207.

Hinze, W. J., Von Frese, R. R., Von Frese, R., & Saad, A. H. (2013). *Gravity and magnetic exploration: Principles, practices, and applications*. Cambridge University Press.

Miller, H. G., & Singh, V. (1994). Potential field tilt—a new concept for location of potential field sources. *Journal of applied Geophysics*, *32*(2-3), 213-217.

Numan, N., & Ghaeb, F. (2019). Geological and Hydrogeological Implications of Gravity Data in the Aqra Plain Iraqi Kurdistan Region. *JJEES*, 145.

Oguama, B. E., Okeke, F. N., & Obiora, D. N. (2021). Mapping of subsurface structural features in some parts of Anambra Basin, Nigeria, using aeromagnetic data. *Modeling*

Earth Systems and Environment, *7*, 1623-1637.

O'Connor, E. "R. Said (ed.) 1990. The Geology of Egypt. x+ 734 pp. Rotterdam, Brookfield: AA Balkema. Price£ 51.00 (hard covers). ISBN 90 6191 856 1." *Geological Magazine* 128.6 (1991): 676-677.

Pham, L. T., Oksum, E., Do, T. D., Nguyen, D. V., & Eldosouky, A. M. (2021). On the performance of phase-based filters for enhancing lateral boundaries of magnetic and gravity sources: a case study of the Seattle Uplift. *Arabian Journal of Geosciences*, *14*, 1-11.

Pick, M., Picha, J., & Vyskocil, V. (1973). Theory of the earth's gravity field. *Amsterdam; New York: Elsevier Scientific Pub. Co*.

Reid, A. B., Allsop, J. M., Granser, H., Millett, A. T., & Somerton, I. W. (1990). Magnetic interpretation in three dimensions using Euler deconvolution. *Geophysics*, *55*(1), 80-91.

Riad, S., & El Etr, H. A. (1985). Bouguer anomalies and lithosphere-crustal thickness in Uganda. *Journal of geodynamics*, *3*(1-2), 169-186.

Roberts H. H and S. P. Murray. (1988). "Gulfs of the Northern Red Sea: Depositional settings of abrupt siliciclastic-carbonate transitions," in Developments in Sedimentology, vol. 42: Elsevier, pp. 99-142.

Saada, S. A. (2020). Delineating the subsurface geological features of the Southern Abu Gharadig Basin, North Western Desert, Egypt, based on gravity and magnetic data. *Geologica Carpathica*, *71*(1).

Saada, S. A., Mickus, K., Eldosouky, A. M., & Ibrahim, A. (2021). Insights on the tectonic styles of the Red Sea rift using gravity and magnetic data. *Marine and*

Petroleum Geology, *133*, 105253.

Safei El-Din, A. (1988). *Geological and hydrogeological studies on the area between Gabal Ataqa and Northern Galala, Egypt* (Doctoral dissertation, Ph. D. Thesis, Fac. Sci., Zagazig Univ. 271p).

Salem, A., Williams, S., Fairhead, D., Smith, R., & Ravat, D. (2008). Interpretation of magnetic data using tilt-angle derivatives. *Geophysics*, *73*(1), L1-L10.

Salem, A. S. (1988). Geological and Hydrogeological Studies on the Area between Gebel Ataqa and Northern Galala Plateau.

Sehsah, H., & Eldosouky, A. M. (2022). Neoproterozoic hybrid forearc–MOR ophiolite belts in the northern Arabian-Nubian Shield: no evidence for back-arc tectonic setting. *International Geology Review*, *64*(2), 151-163.

Spector, A., & Grant, F. S. (1970). Statistical models for interpreting aeromagnetic data. *Geophysics*, *35*(2), 293-302.

Sundararajan, N., Pracejus, B., Ebrahimi, A., Al Hosni, T., & Al Neseiri, J. (2022). Integrated Geophysical Study for Delineation of Structures Favorable to Uranium Mineralization in Al-Amerat, Sultanate of Oman. *Jordan Journal of Earth and Environmental Sciences*, *13*(3), 215-222.

Talwani, M. (1964). Computation of magnetic anomalies caused by two dimensional structures of arbitary shape. *Computers in the mineral industries*, *1*, 464-480.

Tealeb, A., & Riad, S. (1986). Regional gravity anomalies of western Saudi Arabia and their geological significance. *Egyptian Geophysical Society*, *5*, 50-78.

Telford, W. M., Geldart, L. P., & Sheriff, R. E. (1990). *Applied geophysics*. Cambridge university press.

Thompson, D. T. (1982). EULDPH: A new technique for making computer-assisted depth estimates from magnetic data. *Geophysics*, *47*(1), 31-37.

Woollard, G. P. (1959). Crustal structure from gravity and seismic measurements. *Journal of Geophysical Research*, *64*(10), 1521-1544.

Youssef, M. I., & Abd-Allah, A. (2003). Structural geology of the southeastern segment of the Cairo-Suez district, Egypt.

Article in Press: JJEES 16(2), June 2025.

1

2

3

4